MICROMECHANICAL MODELLING OF DUCTILE DAMAGE AND FRACTURE UNDER DYNAMIC LOADING CONDITIONS

N. Jacques, *ENSTA Bretagne, Laboratoire Brestois de Mécanique et des Systèmes (LBMS) – EA 4325, 2 rue François Verny, 29806 Brest cedex 9, France. Téléphone : +33 2 98 34 89 36, Télécopie : +33 2 98 34 87 30, Adresse électronique : nicolas.jacques@ensta-bretagne.fr*

S. Mercier, A. Molinari, C. Czarnota, C. Sartori *Université de Lorraine, Laboratoire d'Etude des Microstructures et de Mécanique des Matériaux (LEM3) – UMR CNRS 7239, Ile du Saulcy, 57045 Metz cedex 01, France*

Keywords : micro-inertia; homogenization; porous materials; ductile damage; dynamic fracture

1. INTRODUCTION

The fracture of ductile materials is often due to the nucleation, growth and coalescence of microscopic voids. Ductile fracture has been the subject on numerous investigations in the past decades [1,2]. On the modelling side, a lot of efforts have been made to develop micromechanical constitutive relationships for porous solids. Gurson [3] performed one of the pioneering works in this direction. The micromechanical approach to ductile fracture (also called local or continuum approach to ductile fracture) is attractive as it makes it possible to link the fracture resistance of a structural component to microstructural details of its constitutive material. Of course, reliable failure predictions require an accurate description of the physical mechanisms governing the void evolution. Recent studies were devoted to the incorporation of void shape effects [4], plastic anisotropy [5,6], matrix tension-compression asymmetry [7] in constitutive relations for porous materials and to the modelling of void coalescence [8-10].

Several researchers employed a micromechanically-based approach to analyse dynamic crack extension [11-14]. In these studies, an extended version of the Gurson-Tvergaard-Needleman (GTN) model accounting for strain-rate sensitivity (viscoplasticity), adiabatic heating due to plastic dissipation and temperature-dependent material properties [15] was used. The GTN model was also applied to the prediction of fracture and fragmentation in dynamic expanding ring experiments [16]. The GTN model is based on the Hill-Mandel homogenization approach, in which the Representative Volume Element (RVE) is assumed to be in static equilibrium. Therefore, in the above-mentioned analyses of dynamic fracture, inertia is only related to the macroscopic motion of the material. This means that void growth and the resulting damage accumulation is tacitly assumed to be dominated by viscous effects. Viscoplastic damage models were also commonly used for the simulation of spall fracture (fracture phenomenon induced by the reflexion of a shock wave on a free surface or an interface) [17-19].

Very high stress levels develop in a material subjected to shock loading or in the vicinity of a running crack. It is well known that, when a voided material is subjected to a sufficiently large tensile stress, void growth may become unstable. This phenomenon, often called cavitation instability, occurs when the release of elastic energy due to the cavity expansion is sufficient to drive the cavity expansion [20-21]. After the onset of unstable cavitation, void growth is unbounded and leads rapidly to the complete fracture of the material. Several studies dedicated to dynamic void expansion revealed that, although material rate dependence influences the early stage of cavity growth, after a short time the void evolution is controlled by micro-inertia (local radial inertia around the expanding void) [22-25]. This raises questions about the applicability of viscoplastic theories of ductile damage which neglect microscale inertia.

The present paper is devoted to the modelling of damage by microvoiding under dynamic loading. In section 2, recent developments on the incorporation of microdynamic effects in continuum damage models are reviewed. In section 3, the accuracy of one of these models is assessed on the basis of

comparisons with dynamic finite element cell computations. In section 4, this model is applied to the simulation of dynamic crack propagation in a double-edge cracked specimen. It is found that microscale inertia greatly affects the computed crack growth behaviour.

2. CONSTITUTIVE MODELLING OF DYNAMIC DAMAGE IN DUCTILE SOLIDS

2.1 Dynamic homogenization techniques

Because of the quasi-static assumption, the use of standard micromechanical approaches to describe the response of porous materials under intense dynamic loading is questionable. In the present section, the dynamic homogenization procedure introduced by Molinari and Mercier [26] is briefly described. They proposed a general formulation for the constitutive modelling of heterogeneous materials, in which inertia effects induced by microscopic motions (local material motions inside the RVE) are taken into account. This approach extends previous works on the dynamic response of voided solids, restricted to isotropic stress states [27-29]. It should be mentioned that Wang and co-workers presented a different formalism to model micro-inertia in heterogeneous materials [30-32].

According to Molinari and Mercier [26], the standard definition of the macrostress as the volume average of the stress field in the RVE is not appropriate for dynamic conditions. Therefore, a new definition of the macroscopic stress $\underline{\underline{\Sigma}}$ was proposed:

$$\underline{\underline{\Sigma}} = \left\langle \underline{\underline{\sigma}} \right\rangle + \left\langle \rho \underline{\gamma_r} \otimes \underline{x_r} \right\rangle \qquad (1)$$

where brackets denote the volume average operator and $\otimes$ the tensorial product. $\underline{\underline{\sigma}}$ stands for the stress field in the RVE. $\underline{\gamma_r}$ and $\underline{x_r}$ represent respectively the acceleration and position of a point in the RVE, relative to the centre of mass of the RVE [33]. Acceleration must be defined with respect to a reference frame. The one considered here should be centred at the centre of mass of the RVE and the axes should remain parallel to the laboratory frame.

The macrostress is the sum of two terms: a static component related to the behaviour of the matrix material and a dynamic component inherited from material accelerations at the microscale:

$$\underline{\underline{\Sigma}} = \underline{\underline{\Sigma}}^{sta} + \underline{\underline{\Sigma}}^{dyn} \qquad (2)$$

Also, it should be noticed that Eq. (1) is exact when homogeneous stress boundary conditions over the RVE are considered. (Of course, Eq. (1) also holds for kinematic boundary conditions. This equation provides a definition of the macroscopic stress which is conjugated to the macroscopic velocity gradient via the principle of virtual power; see Molinari and Mercier (2001)). The rate of macroscopic stress work per unit volume can be written in the following form:

$$\underline{\underline{\Sigma}} : \underline{\underline{L}}^{t} = \left\langle \underline{\underline{\sigma}} : \underline{\underline{d}} \right\rangle + \left\langle \frac{1}{2} \rho \frac{d\left|\underline{v_r}\right|^2}{dt} \right\rangle \qquad (3)$$

where $\underline{\underline{L}}$ is the macroscopic velocity gradient (defined as the volume average of the corresponding microscopic quantity). This relation (3) is the dynamic counterpart of the Hill-Mandel lemma. One sees that the macroscopic stress power is the sum of the volume average of the microscopic stress power and the change of kinetic energy relative to the centre of mass of the RVE.

When the RVE can be represented by a hollow sphere, a closed-form expression for the dynamic stress $\underline{\underline{\Sigma}}^{dyn}$ was obtained by Molinari and Mercier [26] using the extended Hill-Mandel lemma (3) and a trial velocity field almost similar to the Gurson one [3]. In general, the dynamic stress is a tensor, but its spherical component is predominant [34]. Thus, the dynamic stress can be approximated as a dynamic pressure:

$$\underline{\underline{\Sigma}}^{dyn} = P^{dyn} \cdot \underline{\underline{I}} \qquad \textit{with}$$

$$P^{dyn} = \rho_0 a^2 \left[\dot{D}_m \left(f^{-1} - f^{-2/3} \right) + D_m^{\,2} \left(3 f^{-1} - \frac{5}{2} f^{-2/3} - \frac{1}{2} f^{-2} \right) \right] \qquad \textit{and} \qquad D_m = \mathrm{tr}\left(\underline{\underline{L}}\right)/3 \qquad (4)$$

It is interesting to point out that the dynamic pressure is function of the void radius a (internal radius in the hollow sphere). Thus, when microscale inertia is taken into account, the macroscopic response of the material depends on the absolute size of the RVE. From Eq. (4), it appears that the dynamic pressure depends on the strain-rate and its time derivative. Thus, micro-inertia effects give rise, at the macroscale, to additional rate effects with respect to the usual rate sensitivity associated to the viscoplastic response of the matrix material. The case of materials containing non-spherical voids was recently considered [45].

2.2 Statistically Representative Volume Element (RVE) for damaged ductile materials

Microscopic observations of damage in ductile materials generally reveals a broad range of void sizes [35,36]. Therefore, since micro-inertial effects are size-dependent (see Eq. 4), the use of a single hollow sphere as a representative volume is not suitable for dynamic conditions (at least, it does not allow one to describe the effect of void size heterogeneities on the material response). To overcome the limitations of the hollow sphere scheme, it was proposed to consider instead that the material domain contains a population of different-sized voids [34]. Two internal state variables are used to describe the void population: the number of void per unit volume, denoted by N, and the void size distribution function $w(a)$. It should be pointed out that the average porosity in the RVE can be deduced from N and $w(a)$:

$$\tilde{f} = \frac{4}{3}\pi\, N \int_0^{\infty} a^3 w(a) da \qquad (5)$$

It is considered that each void is embedded into a unit cell being represented by a hollow sphere of inner radius a and outer radius b. Thus, the RVE can be viewed as an assemblage of spherical unit cells (Fig. 1). Different assumptions can be made about the distribution of matrix material around each void [37]. For instance, the value of the outer radius can be set identical for all cells. This assumption is probably appropriate when voids are equally-spaced. It is also possible to consider that the local porosity in all cells is equal to the overall porosity. In this case, the cells are homothetic (Fig. 1). From a physical point of view, the homothetic construction is related to the assumption that the local disturbances in the microscopic fields induced by the presence of a void take place in a region whose extent is proportional to the void size.

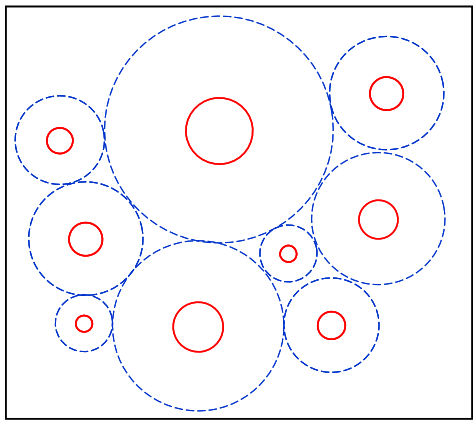

Figure 1. Schematic representation of the Representative Volume Element considered in the present modelling.

The overall material behaviour is obtained by homogenization at two different scales. The first scale corresponds to the unit cell level and the second to the scale of the RVE (aggregate of unit cells). The constitutive response of a given unit cell is described by the dynamic hollow sphere model presented in the previous section, see Eqs. (2,4). The change of scale from the unit cell level to the macroscale can be made in various manners. Two simple homogenization schemes, named D-model and Σ-model, have been tested in [38] in the context of spall fracture. In the D-model, all cells are subjected to the macroscopic strain rate, $\underline{\underline{D}} = \underline{\underline{\tilde{D}}}$. For the Σ-model, the macroscopic stress is

applied to the boundaries of the unit cells, $\underline{\underline{\Sigma}} = \underline{\underline{\tilde{\Sigma}}}$. When the *D*-model is adopted together with the homothetic construction, it can be shown that the macrostress can be expressed as [39]:

$$\underline{\underline{\tilde{\Sigma}}} = \underline{\underline{\tilde{\Sigma}}}^{sta} + \tilde{P}^{dyn} \cdot \underline{\underline{I}} \qquad \textit{with}$$

$$\tilde{P}^{dyn} = \rho_0 \tilde{a}^2 \left[\tilde{\hat{D}}_m \left(\tilde{f}^{-1} - \tilde{f}^{-2/3} \right) + \tilde{D}_m^{\,2} \left(3\tilde{f}^{-1} - \frac{5}{2}\tilde{f}^{-2/3} - \frac{1}{2}\tilde{f}^{-2} \right) \right] \qquad (6)$$

where $\tilde{a}$ is an effective void radius depending on the void size distribution in the material:

$$\tilde{a}^2 = \frac{\int_0^\infty a^5 w(a) da}{\int_0^\infty a^3 w(a) da} \qquad (7)$$

2.3 Example of complete constitutive model

The implementation in a finite element code of constitutive models derived from the micromechanical analysis presented in the previous sections requires some extensions. In particular, elasticity at the macroscopic level is necessary (it is worth noticing that the micromechanical analysis has been developed assuming that the matrix material is incompressible and rigid-perfectly plastic [26]). So, the macroscopic strain rate is considered to be the sum of an elastic part and a plastic part. In the constitutive equations derived from the micromechanical analysis of the previous sections, the strain rate is replaced by the plastic strain rate. The elastic response is described using a hypoelastic relation.

Box 1 provides an overview of an elastic-plastic damage model taking microscale inertia into account, suitable for implementation in a finite element code. The static part of the macroscopic response of the porous material is given by the classical GTN model. It should be noted that void nucleation is not accounted for in the model presented in Box 1 (damage results from the growth of pre-existent voids). The heating due to plastic dissipation is described by considering adiabatic conditions. More details about the derivation of this model can be found in [39]. An extended version of this model, taking void nucleation into account, was recently proposed [46].

Strain-rate tensor:

$$\underline{\underline{\tilde{D}}} = \underline{\underline{\tilde{D}}}^{e} + \underline{\underline{\tilde{D}}}^{p}$$

Elastic response:

$$\overset{\nabla}{\underline{\underline{\tilde{\Sigma}}}} = \frac{E}{1+\nu}\left[\underline{\underline{\tilde{D}}}^{e} + \frac{\nu}{1-2\nu} \mathrm{tr}\left(\underline{\underline{\tilde{D}}}^{e} \right) \cdot \underline{\underline{I}} \right]$$

Dynamic pressure due to micro-inertia effects:

$$\underline{\underline{\tilde{\Sigma}}} = \underline{\underline{\tilde{\Sigma}}}^{sta} + \tilde{P}^{dyn} \cdot \underline{\underline{I}} \qquad \textit{with}$$

$$\tilde{P}^{dyn} = \rho_0 \tilde{a}^2 \left[\tilde{\hat{D}}_m^{p} \left(\tilde{f}^{-1} - \tilde{f}^{-2/3} \right) + \tilde{D}_m^{p\,2} \left(3\tilde{f}^{-1} - \frac{5}{2}\tilde{f}^{-2/3} - \frac{1}{2}\tilde{f}^{-2} \right) \right]$$

$$\tilde{a}^2 = \int_0^\infty a^5 w(a) da \Big/ \int_0^\infty a^3 w(a) da$$

Yield surface (GTN model):

$$\Phi = \left(\frac{\tilde{\Sigma}_{eq}^{sta}}{\bar{\sigma}} \right)^2 + 2q_1 \tilde{f} \cosh\left(\frac{3}{2} q_2 \frac{\tilde{\Sigma}_{m}^{sta}}{\bar{\sigma}} \right) - 1 - \left(q_1 \tilde{f} \right)^2$$

with $\bar{\sigma} = \bar{\sigma}\left(\bar{\varepsilon}, \dot{\bar{\varepsilon}}, T \right)$

Flow rule:

$$\underline{\underline{\tilde{D}}}^{p} = H \frac{\partial \Phi}{\partial \underline{\underline{\tilde{\Sigma}}}^{sta}}$$

Kuhn-Tucker loading/unloading conditions:

$$H \geq 0, \qquad \Phi \leq 0 \qquad H.\Phi = 0$$

Evolution of the internal state variables:

$$\dot{N} = -3N \cdot \tilde{D}_m^p, \qquad \dot{\bar{\varepsilon}} = \frac{\tilde{\underline{\underline{\Sigma}}}^{sta} : \tilde{\underline{\underline{D}}}^p}{\bar{\sigma}\left(1-\tilde{f}\right)}, \qquad \dot{T} = \frac{\beta_{TQ}\bar{\sigma}\,\dot{\bar{\varepsilon}}}{\rho_0 C_0}$$

$$w(a) = \frac{1}{B} w_0\left(\frac{a}{B}\right) \qquad with \qquad B = \exp\left(\int_0^t \frac{\tilde{D}_m^p}{\tilde{f}}\, d\tau\right)$$

Box 1. Constitutive damage model with micro-inertial effects.

3. COMPARISON WITH FINITE ELEMENT CELL COMPUTATIONS

In order to validate the proposed modelling, numerical simulations of a voided unit cell have been carried out with the finite element code ABAQUS/Explicit. A cylindrical cell with an initially spherical void at its centre is subjected to uniaxial deformation (no horizontal displacement at lateral boundaries, see Fig. 2). The initial porosity is equal to 1.5×10^{-4} and the initial void radius is 22 µm (since dynamic conditions are considered, the cell response is size-dependent). The mesh consists of 2085 quadrilateral four-node elements with reduced integration and hourglass control (ABAQUS CAX4R) and 15 triangular constant-strain elements (CAX3). During the cell deformation, very large strains occur in the vicinity the void surface. Thus, adaptive meshing was employed in order to avoid excessive mesh distortion.

The matrix material has an elastic-viscoplastic behaviour obeying to the J_2 flow theory. Adiabatic heating is taken into account. Strain hardening, rate and temperature dependences are described by the following relationship:

$$\bar{\sigma}\left(\bar{\varepsilon},\dot{\bar{\varepsilon}},T\right) = A\left(\varepsilon_0+\bar{\varepsilon}\right)^n \left(1+\left(\frac{\dot{\bar{\varepsilon}}}{\dot{\varepsilon}_0}\right)^m\right)\left(1-\theta^{\nu_T}\right) \qquad with \qquad \theta = \frac{T-T_{ref}}{T_m-T_{ref}} \tag{8}$$

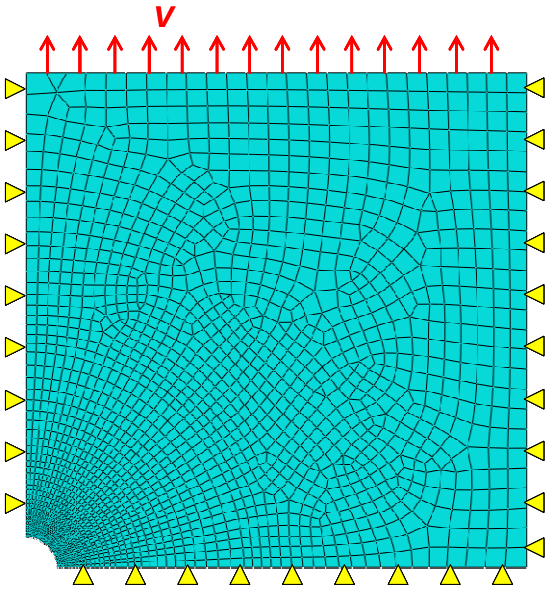

Figure 2. Axisymmetric finite element model of a porous material containing an initially spherical void subjected to uniaxial deformation.

The following parameters, corresponding to some medium-strength steels, are adopted in simulations: $E=2.1\times10^{11}$ Pa, $\nu=0.3$, $\rho_0=7850$ kg/m^3, $A=900\times10^6$ Pa, $\varepsilon_0=0.023$, $n=0.167$, $\dot{\varepsilon}_0=1.86\times10^{-6}$ s^{-1}, $m=0.057$, $T_{ref}=50$ K, $T_m=1773$ K, $\nu_T=0.32$, $C_0=470$ J/kg/K, $\beta_{TQ}=1$. The initial temperature is taken as $T_0=300$ K.

Figure 3 presents a comparison of stress-strain responses derived from the finite element cell computations with results obtained with the present constitutive framework and the GTN model (using $q_1=1.25$ and $q_2=1$ in both cases). In simulations, a constant strain rate is prescribed by adjusting the velocity applied on the top boundary of the cell. Initially, the finite element calculations

predict a step-like stress evolution, due to wave propagation phenomena. Of course, this evolution cannot be predicted by the two constitutive models. Nevertheless, one observes that these wave propagation phenomena are rapidly damped out when the matrix begins to experience plastic deformation.

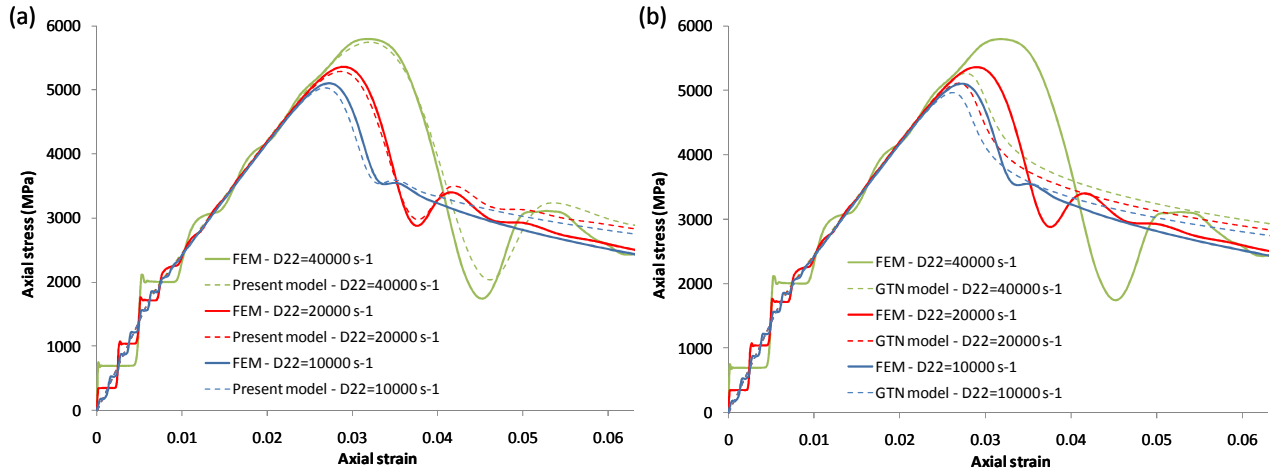

Figure 3. Stress-strain curves for a porous solid in uniaxial deformation at constant strain rate. Comparisons between results of finite element cell computations and predictions of (a) the proposed constitutive model, and (b) the classical GTN model, in which micro-inertia is not taken in account, are depicted.

From Fig. 3, it appears that the present model better describes the cell response than the GTN model, which neglects microscale inertia. The present formulation can accurately capture the evolution of the maximum stress with larger strain rate, while the increase of the peak stress derived from the GTN model is underestimated. In addition, we observe that the stress-strain curves predicted by the finite element simulations exhibit some undulations near the peak stress. These undulations are a signature of micro-inertia [39,40] and become more pronounced when the magnitude of the applied strain rate increases. The present model can reproduce almost perfectly the finite element predictions while the GTN model predicts a monotonic decrease of the axial stress after it reaches its peak value.

In order to investigate the influence of micro-inertia during transient stages, we have also conducted a simulation for a non-constant rate of deformation. The time evolution of the prescribed axial strain rate is given by:

$$\begin{cases} D_{22}(t) = D_0 & , \; t < t_0 \\ D_{22}(t) = D_0 + \dot{D}_0 (t - t_0) & , \; t > t_0 \end{cases} \qquad (9)$$

with D_0 = 10000 s^{-1}, $\dot{D}_0$ = 4.75×10^{11} s^{-2}, t_0 = 4×10^{-6} s. Stress-strain responses obtained with the different models are shown in Fig. 4. The results of the present constitutive model concord with those of the finite element unit cell computations. This is not the case with the GTN model, which is not able to describe the stress evolution in the stage when the strain rate increases.

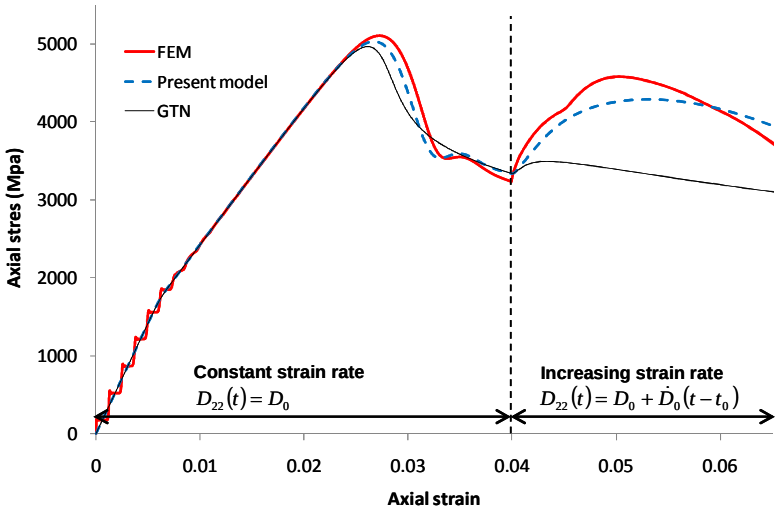

Figure 4. Stress-strain response of a porous material in uniaxial deformation with varying strain rate. Results obtained with the proposed constitutive framework and the GTN model are compared to those of finite element computations. The time evolution of the applied strain rate is given by Eq. (9).

4. APPLICATION TO DYNAMIC CRACK GROWTH

In the present section, the influence of microscale inertia on dynamic crack extension is studied. The proposed model (see Box 1) has been implemented in the finite element code ABAQUS/Explicit via a user-material subroutine. It should be noted that, because of the presence of the time derivative of the plastic strain rate in the constitutive equations, standard integration algorithms [41] cannot be used for the implementation of the present model. Thus, we developed a special implicit constitutive update algorithm based on Newmark's equations. Simulations are performed for a double edge specimen (Fig. 5). Plane-strain conditions are assumed to prevail. A uniform constant surface traction of 1500 MPa is applied on the top and bottom surfaces of the specimen.

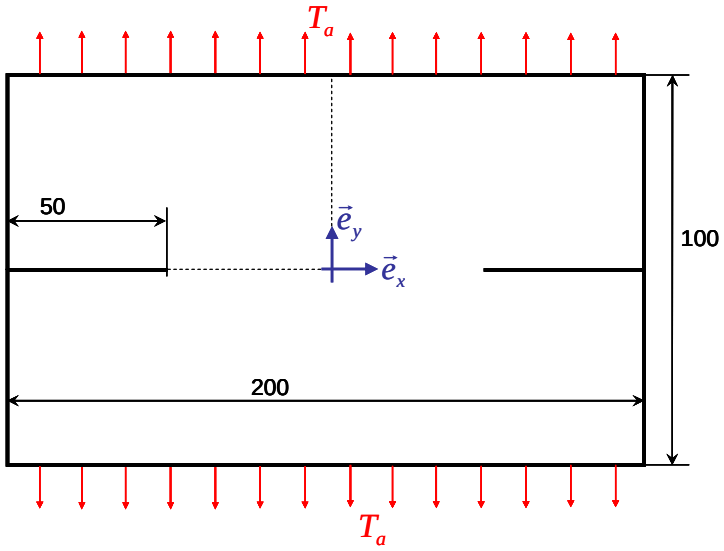

Figure 5. Geometry of the double-edge cracked specimen. Owing to symmetry, only one quarter of the specimen is meshed in simulations.

As suggested by Seaman et al. [36,42] from experimental observations, an exponential function is used to describe the initial void size distribution within the material:

$$w_0(a) = \frac{1}{a_1} exp\left(-\frac{a}{a_1}\right) \qquad (10)$$

This function has a single parameter, denoted by a_1, that corresponds to the initial mean void radius.

The specimen is meshed with four-node elements with reduced integration and hourglass control (CPE4R). In the present simulations, material failure is implemented using the classical element deletion procedure. When a critical porosity f_c is achieved in a particular element, the element is removed from the mesh. Unless otherwise stated, the critical porosity is taken as f_c=0.5. The material parameters related to the matrix behaviour are the same than those adopted in section 3. The initial porosity and mean void radius are respectively equal to 1.5×10^{-4} and 5 µm (the corresponding value of the initial number of voids per unit volume can be calculated using Eqs. 5 and 10: $N_0=4.77\times10^{10}$ m^{-3}). The Tvergaard parameters are set as q_1=1.5 and q_2=1.15 [43].

Simulations revealed a significant role of microscale inertia. In particular, it was found that micro-inertia yields a regularizing effect. Computations based on the present model exhibit much less mesh sensitivity than those based on a viscoplastic version of the GTN model (it should be noted than the GTN model is the limit of the proposed one as the initial void radius a_1 tends to 0, for a given initial porosity). Figure 6 displays contours of porosity predicted by the GTN model (that neglects microscale inertia) for two levels of mesh refinement. It is seen that porosity concentrates in a narrow region, whose size depends on mesh resolution. In fact, the thickness of this narrow band is equal to the element height. Furthermore, at the considered time, the crack has run over a longer distance with the fine mesh, showing that the crack growth behaviour predicted by the GTN model is mesh-sensitive. Figure 7 represents the damage distribution in the specimen predicted by the present model for several mesh densities. It is seen that damage is spread over an area that does not depend on the mesh size. Besides, the amount of crack advance achieved at the considered time is independent on the mesh size. Microscale inertia avoids spurious mesh effects. It was shown that this regularizing effect is related to the enhanced strain-rate sensitivity of the constitutive response at the scale of the RVE due to micro-inertia [39] (By enhanced strain rate sensitivity, it is meant that microscale inertia gives rise to additional rate effects at the macroscale. However, it should be noted that micro-inertia effects are mainly related to the time derivative on the plastic strain rate).

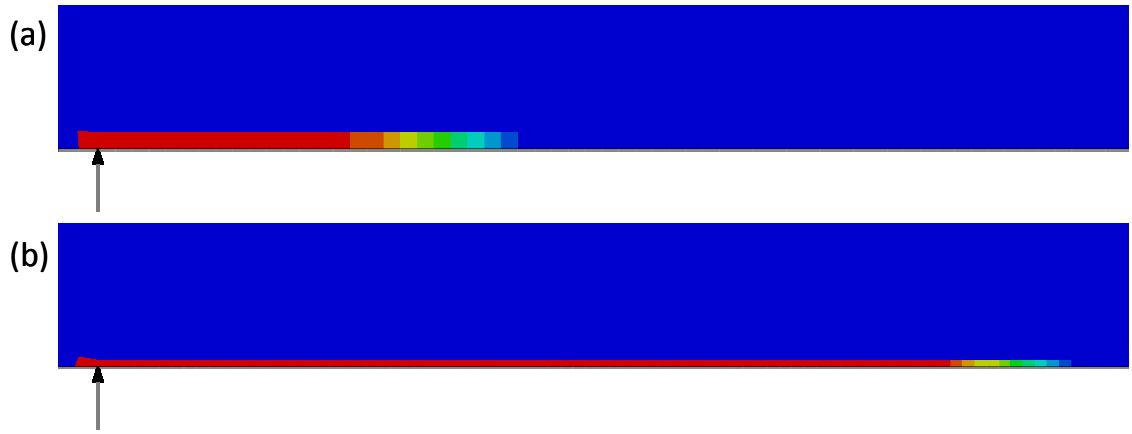

Figure 6. Effect of the mesh size on the porosity distribution (plotted on the undeformed configuration) in the vicinity of the initial position of the crack tip (indicated by an arrow) at t = 9.6 µs. Simulations were carried out with the ***GTN model****. Colour map: 1.5×10^{-4} (blue) ≤ porosity ≤ 0.5 (red). The extent of the region depicted in this figure is about 0.63×0.082 mm^2. (a) coarse mesh (element size in the crack tip region:10×10 μm^2); (b) medium mesh (7.25×5 μm^2).*

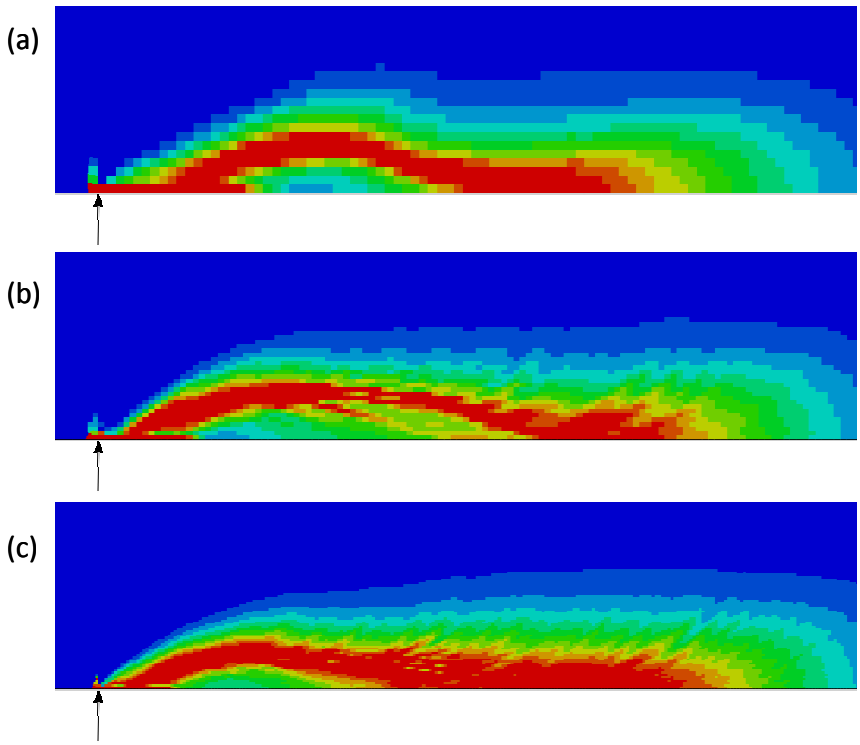

*Figure 7. Effect of the mesh size on the porosity distribution (plotted on the undeformed configuration) in the vicinity of the initial position of the crack tip (indicated by an arrow) at t = 15 µs. Simulations were carried out with the **present model**. The colour map is as in Fig. 6. The size of the region shown in this figure is about 0.87×0.22 mm^2. (a) coarse mesh (element size in the crack tip region:10×10 µm^2); (b) medium mesh (7.25×5 µm^2); (c) fine mesh (3.625×2.5 µm^2).*

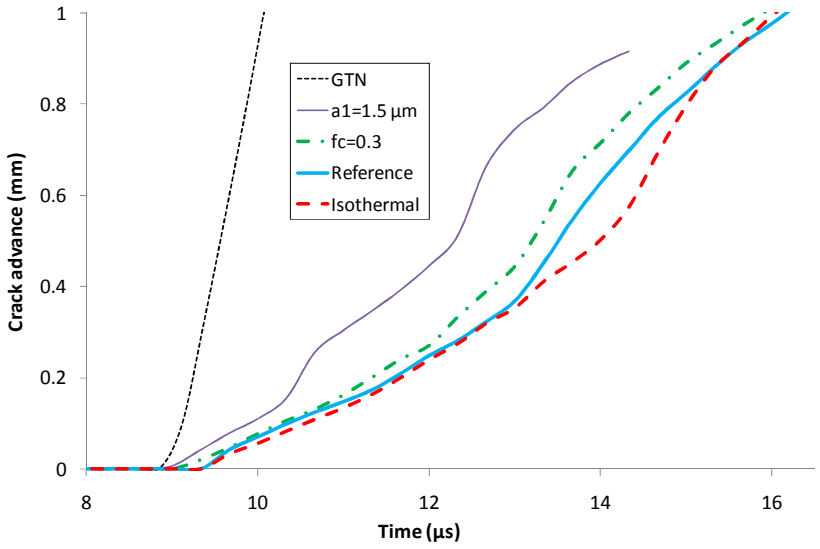

Figure 8. Effect of various parameters on the predicted crack growth behaviour. The reference curve is obtained with the material parameters given at the beginning of section 4.

The effect of several material parameters on the crack growth behaviour is analyzed in Fig. 8. The reference curve corresponds to the set of material parameters given at the beginning of the present section (in particular, a_1=5 µm and f_c=0.5). To illustrate the role of microscale inertia, crack advance versus time curves obtained with a_1=1.5 µm and with the GTN model (that corresponds to a_1=0) are plotted in Fig. 8. It is reminded that micro-inertia effects become more pronounced when the initial mean void radius increases, see Eq. 6. It appears that micro-inertia strongly influences the speed at which the crack propagates. For the reference case, the average velocity on the first 0.8 mm of crack advance is 146 m/s. It is equal to 180 m/s for a_1=1.5 µm and 784 m/s when micro-inertia is not

accounted for (GTN model). On the other hand, crack extension is not significantly affected by a change of the value of the critical porosity (fracture criterion). Indeed, the mean crack speed increases only from 146 to 153 m/s when the critical porosity f_c is taken as 0.3 instead of 0.5. Dynamic ductile crack growth involves high strain rate deformation and causes an adiabatic heating of the specimen. Simulations predict a temperature rise as high as 500°C in the vicinity of the crack tip. However, it seems that thermal effects do not very much influence the crack growth behaviour. Indeed, the crack advance versus time curves obtained by considering adiabatic and isothermal conditions are almost similar for the considered configuration (Fig. 8).

5. CONCLUSION

In this paper, a micromechanical model for dynamic damage due to void growth in ductile media is presented. As compared to standard Gurson-like models, the original feature of the proposed approach is that microscale inertia is taken into account. Micro-inertia effects have been incorporated using an extended, dynamic version of Hill-Mandel's homogenization approach and are a direct consequence of local material accelerations around the growing voids.

Comparison between theoretical predictions derived from the proposed model and results of dynamic finite element cell computations shows a good agreement. Indeed, the present constitutive model better describe the cell response than the standard GTN one, especially during transient stages when rapid strain rate variations occur.

The proposed constitutive model was employed to simulate dynamic crack extension. The effect of microscale inertia is found to be significant. In particular, micro-inertia limits the speed at which cracks propagate. Also, it was observed that micro-inertia provides a regularizing effect. Thus, numerical simulations based on the present model do not suffer from pathological mesh sensitivity. Given this reduced mesh dependency, one may ask whether the incorporation of micro-inertia in continuum theories of ductile fracture negates the need to resort to non-local damage models. For the time being, there is no definite answer to that question. Obviously, the regularizing effect of micro-inertia vanishes under quasi-static conditions. Therefore, simulations of stable crack growth based on the present model will be clearly mesh-dependent. For quasi-static problems, the use of non-local formulations is necessary to prevent spurious mesh effects. In the case of dynamic loadings, microscale inertia yields a regularizing effect. However, it is possible that there could exist an interplay between micro-inertia and non-local effects. This point will be the subject of a future work.

In previous works [38,44], a damage model dedicated to the simulation of spall fracture was developed using the present methodology. Comprehensive comparisons between numerical calculations and experiments (plate impact tests) were carried out. The modelling was found to be able to accurately describe damage development and free surface velocity profiles for various test conditions. Furthermore, it was shown that the accuracy of the numerical simulations is strongly related to micro-inertia [44]. The present contribution suggests that micro-inertia must also be taken into account to analyse crack propagation under dynamic loading. However, comparisons between modelling and experiments for dynamic crack growth problems are needed to confirm these findings.

REFERENCES

[1] Benzerga AA, Leblond J-B. Ductile fracture by void growth to coalescence. *Adv Appl Mech* 2010;**44**:169-305.

[2] Besson J. Continuum models of ductile fracture: a review. *Int J Damage Mech* 2010;**19**:3-52.

[3] Gurson AL. Continuum theory of ductile rupture by void nucleation and growth. Part I: yield criteria and flow rules for porous ductile media. *J Eng Mater Technol* 1977;**99**:2-15

[4] Gologanu M, Leblond J-B, Perrin G, Devaux J. Recent extensions of Gurson's model for porous ductile metals. In: Suquet P., editor, *Continuum Micromechanics*, New-York; CISM Lectures Series. Springer; 1997, p. 61–130.

[5] Benzerga AA., Besson J. Plastic potentials for anisotropic porous solids. *Eur J Mech A/Solids* 2001;**20**:397–434..

[6] Keralavarma SM, Benzerga AA. A constitutive model for plastically anisotropic solids with non-spherical voids. *J Mech Phys Solids* 2010;**58**:874–901.
[7] Cazacu O, Stewart JB. Analytical plastic potential for porous aggregates with matrix exhibiting tension-compression asymmetry. *J Mech Phys Solids* 2009;**57**:325-341.
[8] Gologanu M, Leblond J-B, Perrin G, Devaux J. Theoretical models for void coalescence in porous ductile solids – I: Coalescence in "layers". *Int J Solids Struct* 2001;**38**:5581–5594.
[9] Benzerga AA. Micromechanics of Coalescence in Ductile Fracture. *J Mech Phys Solids* 2002;**50**:1331–1362.
[10] Leblond JB, Mottet G. A theoretical approach of strain localization within thin planar bands in porous ductile materials. *CR Mecanique* 2008;**336**:176-189.
[11] Needleman A, Tvergaard V. An analysis of dynamic, ductile crack growth in a double edge cracked specimen. *Int J Fract* 1991;**49**:41-67.
[12] Needleman A, Tvergaard V. A numerical study of void distribution effects on dynamic, ductile crack growth. *Eng Fract Mech* 1991;**38**:157-173.
[13] Needleman A, Tvergaard V. Mesh effects in the analysis of dynamic ductile crack growth. *Eng Fract Mech* 1994;**47**:75-91.
[14] Xia L, Cheng L. Dynamic ductile crack growth and transition to cleavage – a cell model approach. *Int J Fract* 2000;**102**:155-175.
[15] Tvergaard V, Needleman A. An analysis of the temperature and rate dependence of Charpy V-notch energies for a high nitrogen steel. *Int J Fract* 1988;**37:**197–215.
[16] Becker R. Ring fragmentation predictions using the Gurson model with material stability conditions as failure criteria. *Int J Solids Struct* 2002;**39**:3555-3580.
[17] Rajendran AM, Dietenberger MA, Grove DJ. A void growth-based failure model to describe spallation. *J Appl Phys* 1988;**85**:1521-1527.
[18] Eftis J, Nemes JA, Randles PW. Viscoplastic analysis of plate impact spallation. *Int J Plast* 1991;**7**:15-39.
[19] Addessio FL, Johnson JN. Rate-dependant ductile failure model. *J Appl Phys* 1993;**74**:1640-1648.
[20] Huang Y, Hutchinson JW., Tvergaard V. Cavitation instabilities in elastic–plastic solids. *J Mech Phys Solids* 1991;**39**:223–241.
[21] Tvergaard V, Huang Y, Hutchinson JW. Cavitation instabilities in a power hardening elastic–plastic solid. *Eur J Mech A/Solids* 1992;**11**:215–231.
[22] Ortiz M, Molinari A, 1992. Effect of strain hardening and rate sensitivity on the dynamic growth of a void in a plastic material. *J Appl Mech* 1992;**59**:48-53.
[23] Tong W, Ravichandran G. Inertia effects on void growth in porous viscoplastic materials. *J Appl Mech* 1995;**62**:633-639.
[24] Wu XY, Ramesh KT, Wright TW. The dynamic growth of a single void in a viscoplastic material under transient hydrostatic loading. *J Mech Phys Solids* 2003;**51**:1-26.
[25] Wright TW, Ramesh KT. Statistically informed dynamics of void growth in rate dependant materials. *Int J Impact Eng* 2009;**36**:1242-1248.
[26] Molinari A, Mercier S. Micromechanical modelling of porous materials under dynamic loading. *J Mech Phys Solids* 2001;**49**:1497-1516.
[27] Carroll MM, Holt AC. Static and dynamic pore-collapse relations for ductile porous materials. *J Appl Phys* 1972;**43**:1626–1636.
[28] Johnson JN. Dynamic fracture and spallation in ductile solids. *J Appl Phys* 1981;**52**:2812–2825.
[29] Cortes R. The growth of microvoids under intense dynamic loading. *Int J Solids Struct* 1992;**29**:1339–1350..
[30] Wang ZP. Void-containing nonlinear materials subject to high-rate loading. *J Appl Phys* 1997;**81**:7213–7227.
[31] Wang ZP, Jiang Q. A yield criterion for porous ductile media at high strain rate. *J Appl Mech* 1997;**64**:503–509.

[32] Wang ZP, Sun CT. Modeling micro-inertia in heterogeneous materials under dynamic loading. *Wave Motion* 2002;**36**:473–485.
[33] Wright TW, Ramesh KT. Dynamic void nucleation and growth in solids: A self-consistent statistical theory. *J Mech Phys Solids* 2008;**56**:336-359.
[34] Dragon A, Trumel H. Damage under impact loading – some modelling challenges. In: *5th International Symposium High Dynamic Pressure*, Saint-Malo, France, CEA; 2003, p. 267-283.
[35] Becker R, Needleman A, Richmond O, Tvergaard V. Void growth and failure in notched bars. *J Mech Phys Solids* 1988;**36**:317-351.
[36] Antoun T, Seaman L, Curran DR, Kanel G, Razorenov S, Utkin A. *Spall Fracture*. Berlin: Springer; 2003.
[37] Czarnota C. *Endommagement ductile des matériaux métalliques sous chargement dynamique - Application à l'écaillage*. PhD thesis, University of Metz; 2003. (In French).
[38] Czarnota C, Jacques N, Mercier S, Molinari A. Modelling of dynamic fracture and application to the simulation of plate impact tests on tantalum. *J Mech Phys Solids* 2008;**56**:1624-1650.
[39] Jacques N., Mercier S., Molinari A. Effects of microscale inertia on dynamic ductile crack growth. *J Mech Phys Solids* 2012, 60 :665-690.
[40] Weinberg K, Mota A, Ortiz M. A variational constitutive model for porous metal plasticity. *Comput Mech* 2006;**37**:142-152.
[41] Simo JC, Hughes TJR. *Computational Inelasticity*. New-York: Springer-Verlag, 1998.
[42] Seaman L, Curran DR, Shockey DA. Computational models for ductile and brittle fracture. *J Appl Phys* 1976;**47**:4814-4826.
[43] Besson J, Steglich D, Brocks W. Modeling of crack growth in round bars and plane strain specimens. *Int J Solids Struct* 2001;**38**:8259-8284.
[44] Jacques N, Czarnota C, Mercier S, Molinari A. A micromechanical constitutive model for dynamic damage and fracture of ductile materials. *Int J Fract* 2010;**162**:159-175.
[45] Sartori C., Mercier S., Jacques N., Molinari A. Constitutive behavior of porous ductile materials accounting for micro-inertia and void shape. *Mech. Mat.* 2015;**80**:324-339.
[46] Jacques N., Mercier S., Molinari A. A constitutive model for porous solids taking into account microscale inertia and progressive void nucleation. *Mech. Mat.* 2015;**80**:311-323.